TIME-TEMPERATURE-TRANSFORMATION DIAGRAM OF ALLOY 725

Sarwan Mannan and Frank Veltry
Special Metals Corporation
3200, Riverside Drive, Huntington, WV 25705

Abstract

Commercially produced INCONEL® alloy 725 was annealed and heat-treated in the temperature range of 650°C to 1093°C for the times of 15 minutes to 100 hours. Heat-treated specimens were tested for hardness and room temperature tensile properties. To develop an understanding of the observed mechanical properties, tested specimens were examined using optical metallography, scanning electron microscopy, transmission electron microscopy, and X-ray diffraction. Data generated from these analytical techniques is presented in the form of a time-temperature-transformation diagram.

® INCONEL is a registered trademark of the Special Metals Corporation group of companies

Introduction

INCONEL® Alloy 725 is a highly corrosion resistant nickel-based alloy which can be age-hardened to strength levels comparable to alloys 706 and 718 by the precipitation of intermetallic phases γ"{Ni3(NbAlTi}, and γ' {Ni3(AlTi} [1-2]. This combination of high strength, ductility, and excellent corrosion resistance make the alloy attractive for turbine applications and also for use in other challenging environments such as sea water, deep sour gas wells, and mineral acids [3].

Mechanical properties and corrosion resistance are governed by the microstructure. To tailor the microstructure for properties, an understanding of phase stability with time and temperature is essential. In this study, commercially produced material was annealed at 1149°C for 2 hours and heat-treated in the temperature range of 650°C to 1093°C for the times of 15 minutes to 100 hours. This was followed by hardness and room temperature tensile testing. Tested specimens were examined using optical metallography, scanning electron microscopy (SEM), transmission electron microscopy (TEM), and X-ray diffraction (XRD) analyses. Data generated using these analytical techniques is presented in the form of a time-temperature-transformation diagram.

Experimental Procedure

A commercial heat of alloy 725 produced by vacuum induction melting and vacuum arc remelting was forged to 152 x 203mm billets which were hot rolled to 25.4mm diameter rod. Specimens were cut from the rod, annealed in the lab at 1149°C for 2 hours, and air cooled. Annealed specimens were heat-treated in the temperature range of 650°C to 1093°C for the times of 15 minutes to 100 hours and tested for hardness and room temperature tensile properties. Hot rolled material was also heat treated at 871°C and 927°C and their microstructure was characterized. Chemical composition of the material is given in Table I.

Table I. Chemical Composition (wt%)

Ni	Cr	Mo	Fe	Nb	Ti	Al	C	N	Mn	S
58.3	20.8	8.0	7.4	3.5	1.52	0.21	0.006	0.008	0.07	0.0004

Optical Metallography and X-Ray Diffraction:

A two-stage procedure was found suitable to reveal the microstructure. It involved dipping the specimen in concentrated HCl for 5 seconds and immersing in 1% Br/CH₃OH solution for 15-20 seconds. Selected specimens were electrolytically etched with a solution containing 60ml H₃PO₄, 16ml H₂SO₄, 10g of CrO₃, and 12ml of H₂O. Polished specimens were subjected to electrolytic extraction in CH₃OH/HCl and/or Phosphoric acid solution at 0.5A for 4-20 hours using standard ASTM practice E963-83. The extracted residue was subjected to XRD, SEM, and Energy Dispersive X-Ray (EDX) analyses.

Transmission Electron Microscopy:

To prepare specimens for TEM, 400-500μm thick foils were cut with a precision saw. The 3mm discs were mechanically punched from the foils and ground to 150-200μm. The discs were then electrolytically polished by a twin jet thinning apparatus using a solution of 10% perchloric acid in methanol at 28V and at −50°C. Thin foils were examined with a Phillips EM 400 microscope.

Results and Discussion

Hardness and Tensile Properties:
Figure 1 shows Time-Temperature-Hardness (TTH) curve for the specimens exposed in the temperature range of 649°C to 1093°C for the time of 15 minutes to 100 hours. It should be mentioned that hardness was determined on Rockwell B and C scales and converted to Vickers Hardness Numbers to have one hardness scale on the plot. The degree of precipitation strengthening is highest in the temperature range of 760°C to 816°C, Figure 1.
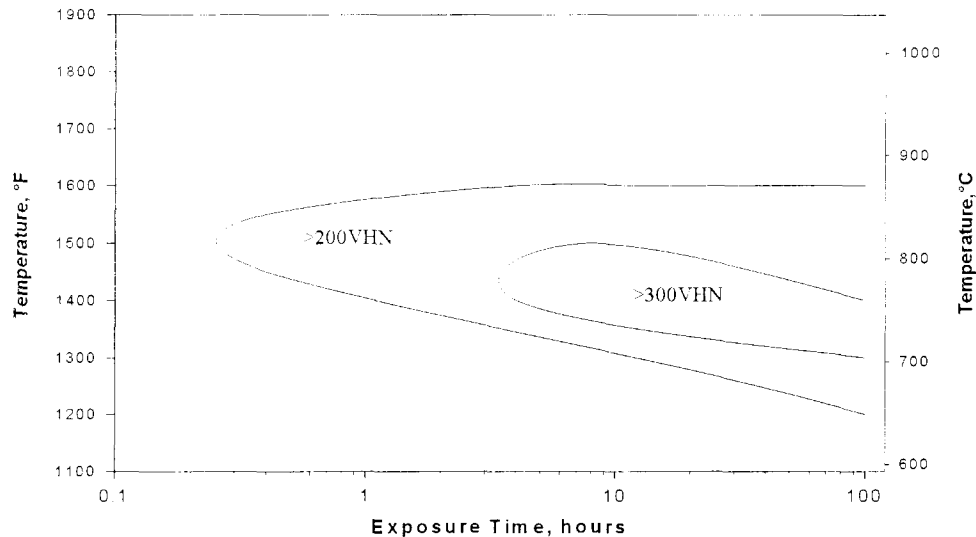

Figure 1: Time Temperature Hardness plot of the material annealed at 1149°C for 2h and air-cooled prior to the heat treatments.

Yield strength and elongation for the specimens exposed at 760°C and 871°C are shown in Figures 2a and 2b. Yield strength for 760°C/100h exposure is roughly double that of 871°C/100h. However, the elongation for the former is half that of latter. Metallographic analyses were carried out to understand the hardness and tensile properties.
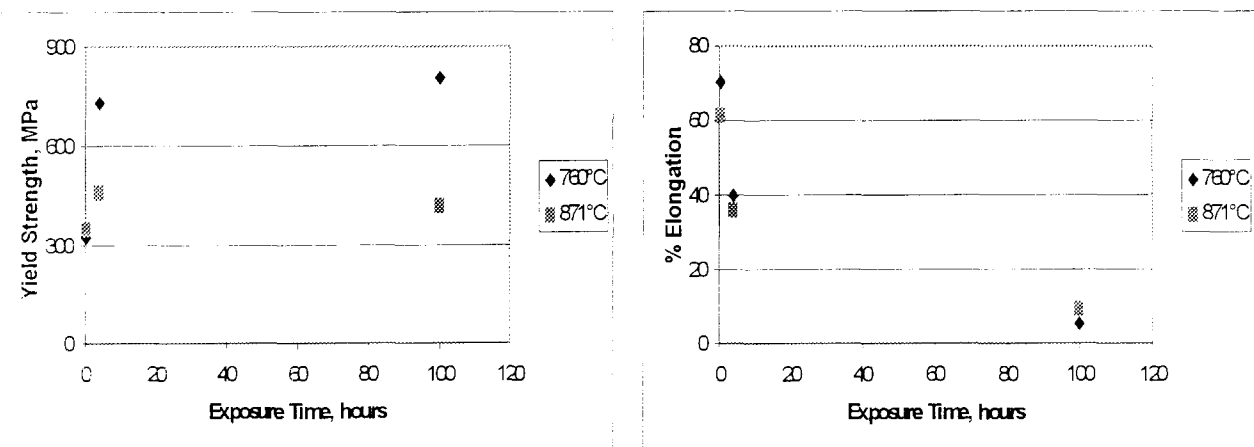

Figure 2: Yield strength and elongation of the specimens exposed at 760°C and 871°C.

Optical and Scanning Electron Microscopy:

The grain size of the material annealed at 1149°C for 2 hours was ASTM #00. Annealed material contained TiN and MC carbides [Ti and (TiNb) carbides] which are typically found in some superalloys [4,5]. No additional precipitation could be observed on exposure at 649°C. On prolonged exposure at 704°C, grain boundary precipitates were observed.

Figures 3 shows photographs of the specimens exposed at 760°C for 4, 25, and 100 hours. At 4 hours exposure time, only partial coverage of grain boundary precipitates is observed. On increasing the exposure time to 25 hours, the grain boundaries are essentially covered with precipitates. At 100h exposure, grain boundaries are fully covered with heavy precipitates and the matrix has a mottled appearance typical of overaged γ'/γ'' [6]. Specimens exposed at 816°C for 4, 25, and 100 hours also show grain boundary precipitates and intragranular mottled appearance, Figure 4.

Exposures at 871°C for 4h and 25h result in grain boundary precipitates and intragranular mottled appearance, Figure 5a and 5b. However, on 100 hours heat treatment, additional inter and intragranular acicular recipitates are observed, Figure 5c. An exposure at 927°C for 4h revealed grain boundary precipitates only, Figure 6a. However, on increasing the exposure time at 927°C to 25h and 100h, inter- and intragranular acicular precipitates were observed, Figure 6b and 6c. Volume fraction and size of the acicular precipitates for 100h exposure is larger than 25h exposure. Absence of intragranular mottled appearance suggests that γ'/γ'' precipitates are in solution at 927°C. On increasing the exposure temperature to 982°C, the material contained only intergranular precipitates, Figure 7.
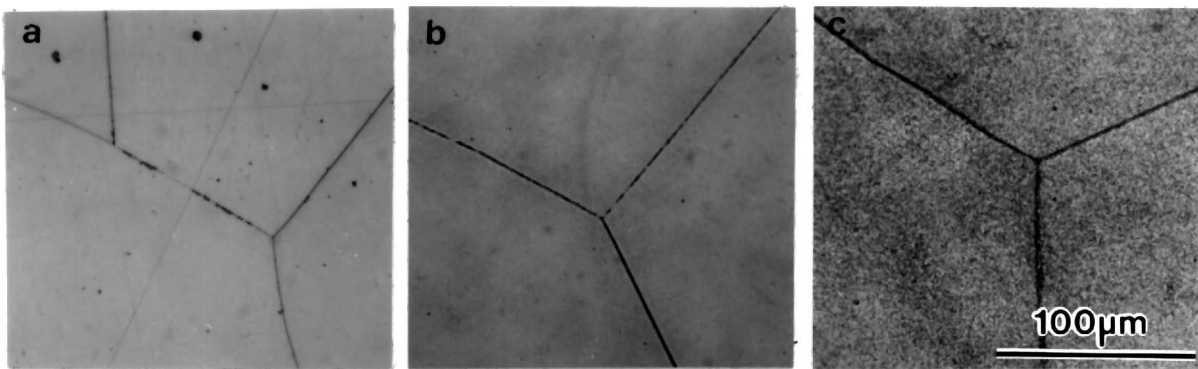

Figure 3: Microstructure of the specimens exposed at 760°C: a) 4h, b) 25h, and c) 100h
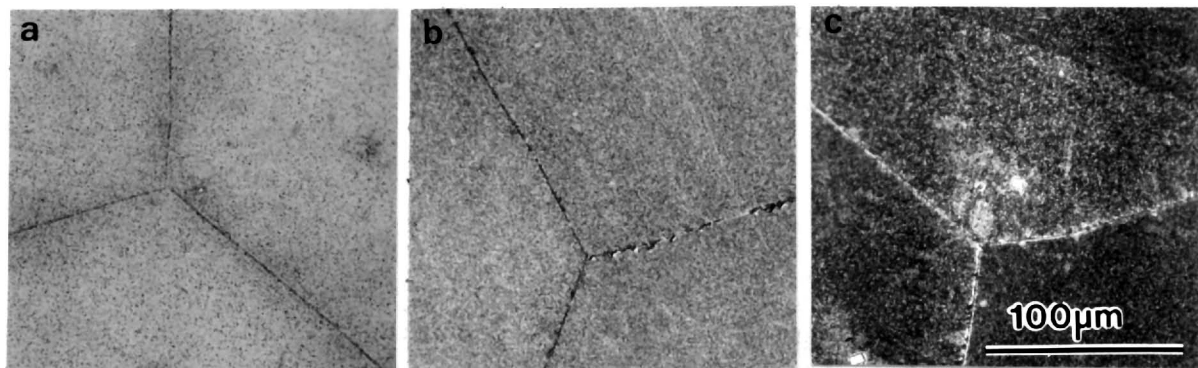

Figure 4: Microstructure of the specimens exposed at 816°C: a) 4h, b) 25h, and c) 100h
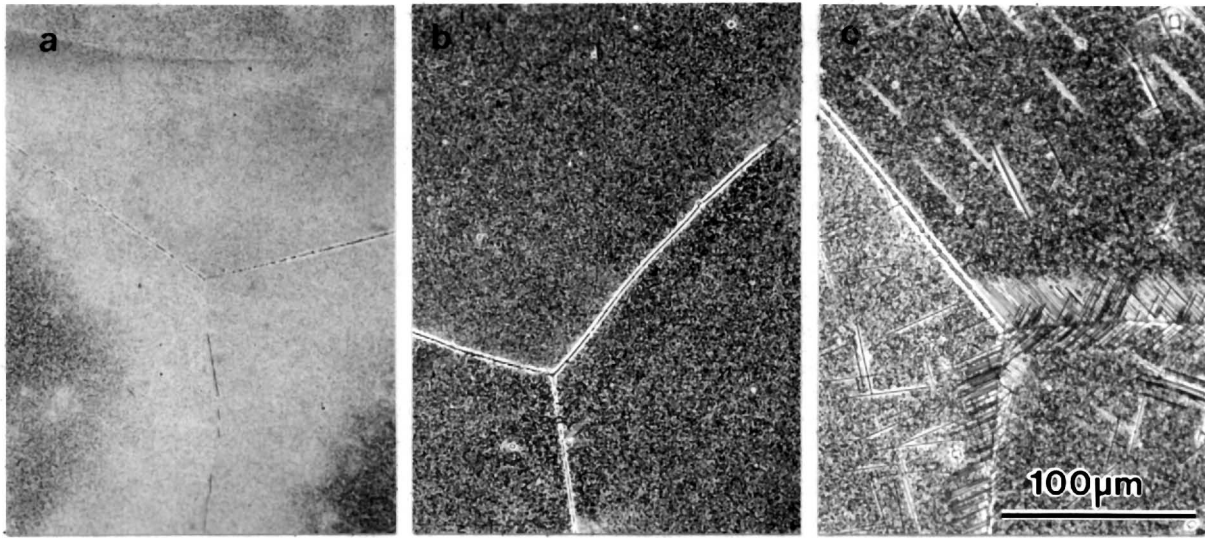
Figure 5: Microstructure of the specimens exposed at 871°C: a) 4h, b) 25h, and c) 100h
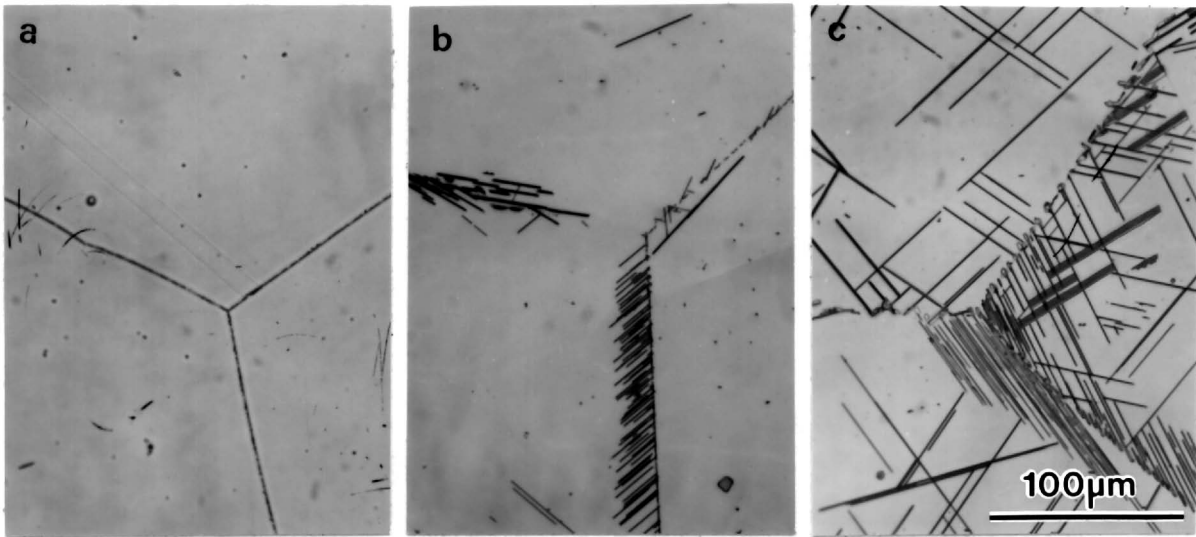

Figure 6: Microstructure of the specimens exposed at 927°C: a) 4h, b) 25h, and c) 100h
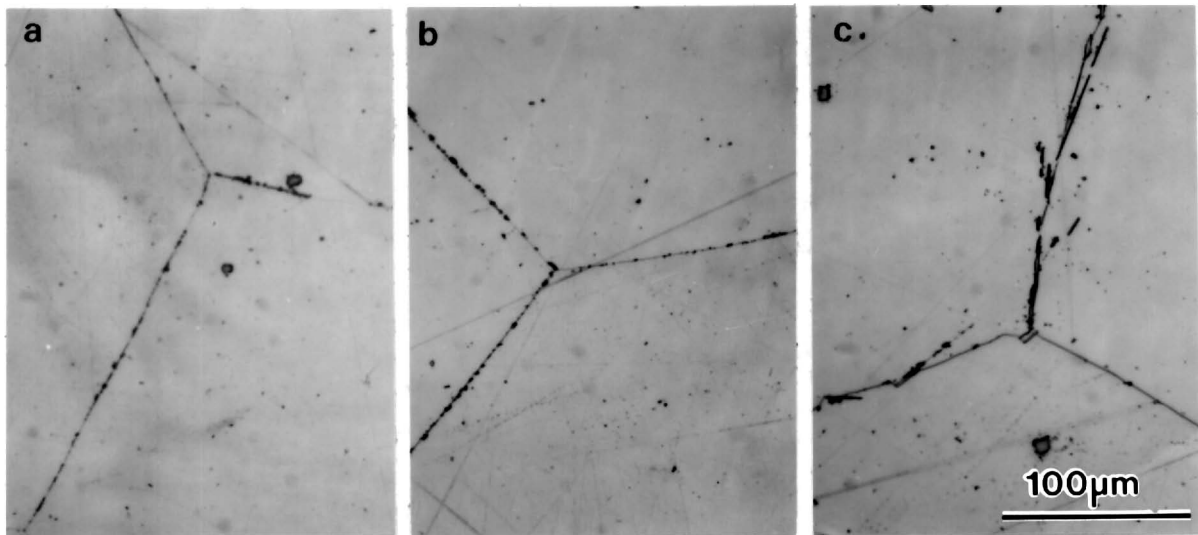

Figure 7: Microstructure of the specimens exposed at 982°C: a) 4h, b) 25h, and c) 100h

Figure 8 shows size and morphology of γ'/γ'' precipitates in the specimens exposed at 871°C for 4h, 25h, and 100h. To reveal the effect of temperature on precipitation kinetics, photomicrographs of the specimens exposed for 100h at 760°C and 816°C are also shown. These SEM photomicrographs also show an acicular intergranular phase for 871°C/25h and 816°C/100h exposures, which could not be revealed by optical microscopy, Figures 3 and 4.
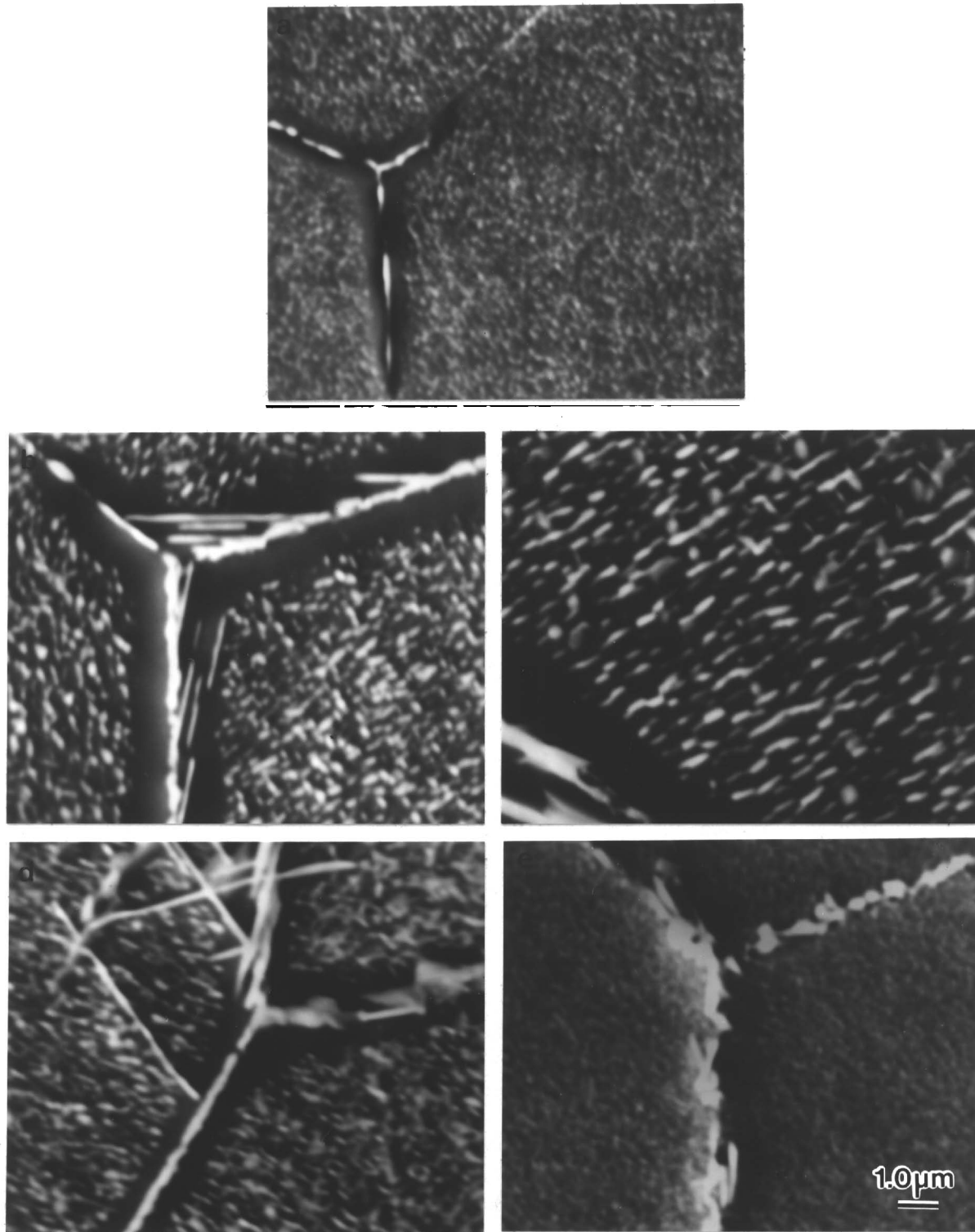

Figure 8: SEM photomicrographs of the exposed specimens. a) 871°C/4h, b) 871°C/25h, c) 871°C/100h, d) 816°C/100h, and e) 760°C/100h.

XRD and TEM Analyses:

The extracted residues from all specimens contained matrix grain fragments, TiN, and MC (Ti, Nb) carbides. Figures 9a to 9c show morphology and EDX patterns of Ni_3Ti-type η precipitates formed at 927°C. Due to the dilution of the X-rays collected from a large matrix area, the EDX patterns from thin needle-like η precipitates and matrix are similar, Figures 9b and 9c. However, EDX pattern from the extracted residue showed definite enrichment in Ti and Ni, Figure 10. The X-Ray diffraction pattern from the residue was similar to JCPDF # 23-1275. Figure 11 shows morphology and EDX pattern of σ phase from the extracted residue of specimen annealed at 1149°C for 2h and exposed at 927°C for 50h. Grain boundary $M_{23}C_6$ type carbide morphology and EDX pattern is shown in Figures 12a and 12b. It shows enrichment of Cr and Mo as compared to the matrix shown in Figure 9c. Selected TEM analyses were conducted to confirm the findings of X-Ray diffraction analysis. Sigma phase in a specimen exposed at 927°C for 15 minutes in the hot worked condition is shown in Figure 13. Also, γ'' in the specimen annealed at 1149°C for 2h and exposed at 760°C for 12h is shown in Figure 14.
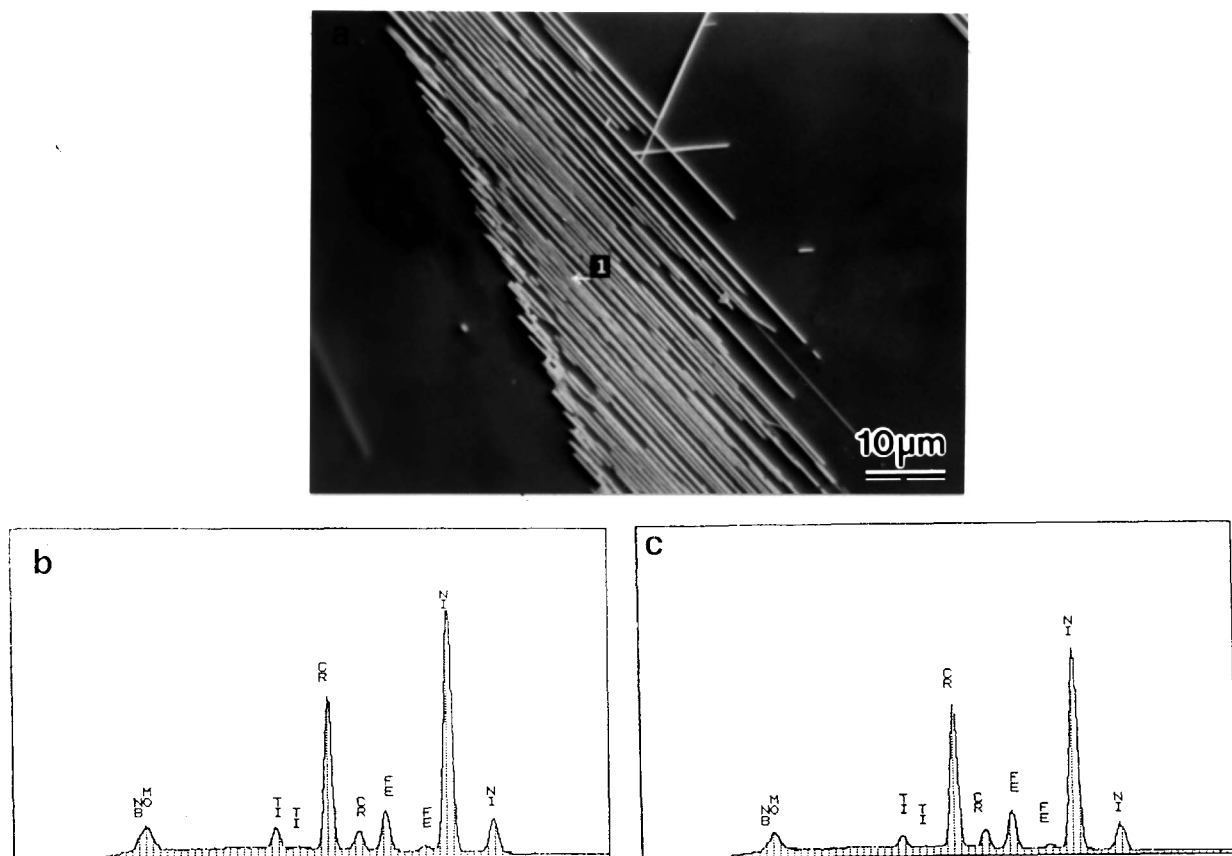

Figure 9: SEM/EDX analysis of the specimen annealed at 1149°C for 2h and exposed at 927°C for 100h. a) SEM photomicrograph, b) EDX pattern of the matrix, c) EDX pattern from site 1.
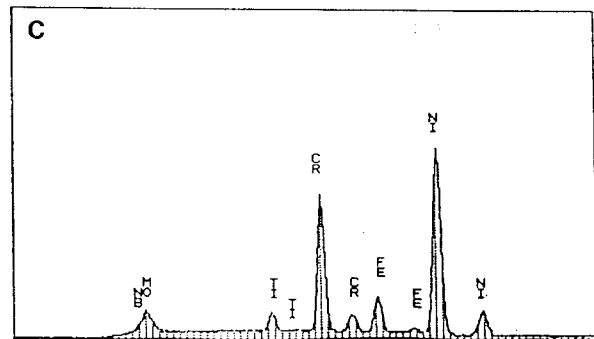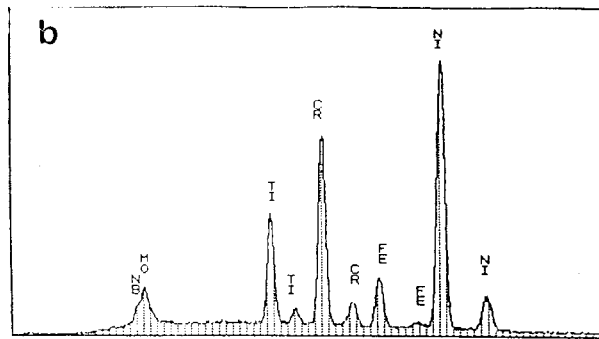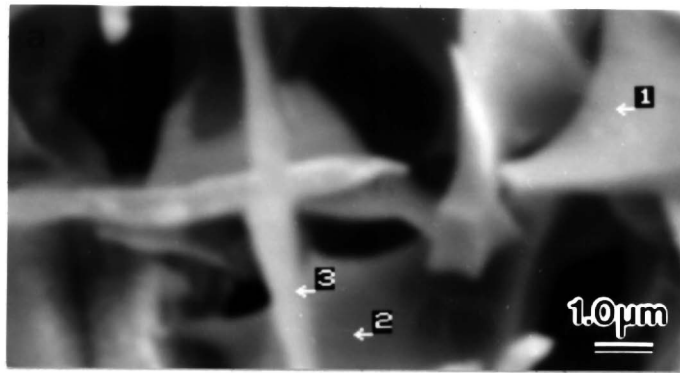
351

Figure 10: SEM/EDX analysis of the residue extracted from the specimen annealed at 1149°C for 2h and exposed at 927°C for 12h. a) SEM photomicrograph, b) EDX pattern from site 1, c) EDX pattern from site 1.
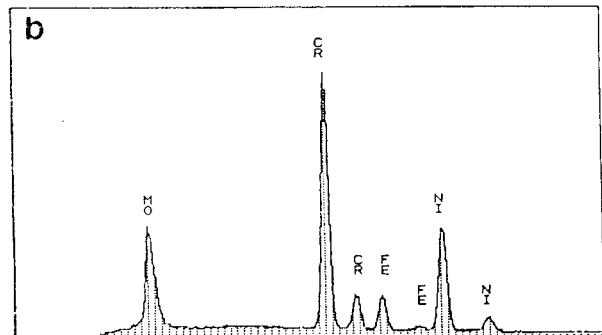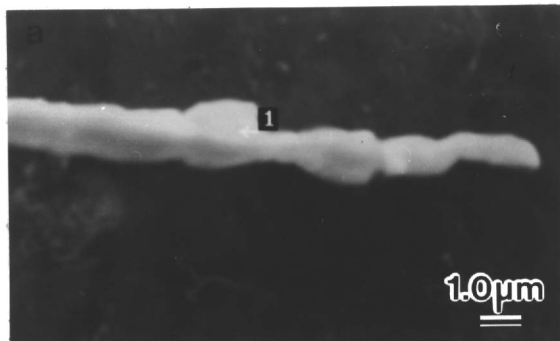

Figure 11: SEM photomicrograph and EDX pattern of σ phase from the extracted residue of the specimen annealed at 1149°C for 2h and exposed at 927°C for 50h. The X-Ray diffraction was similar to JCPDF # 9-284
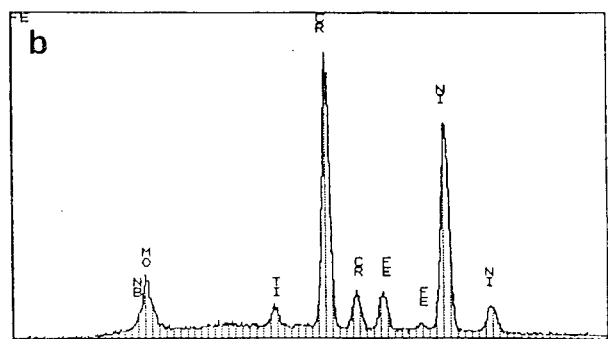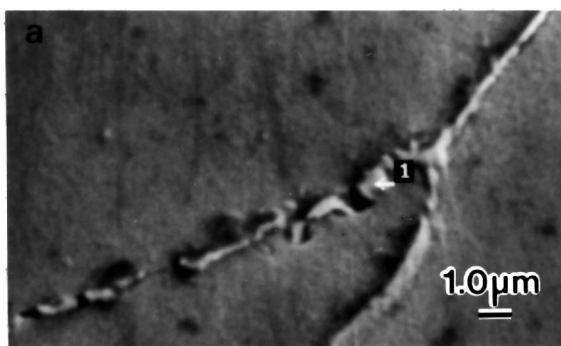

Figure 12: SEM photomicrograph and EDX pattern of $M_{23}C_6$ carbide phase from the specimen annealed at 1149°C for 2h and exposed at 760°C for 100h. The X-Ray diffraction pattern from the extracted residue was similar to JCPDF # 5-980.
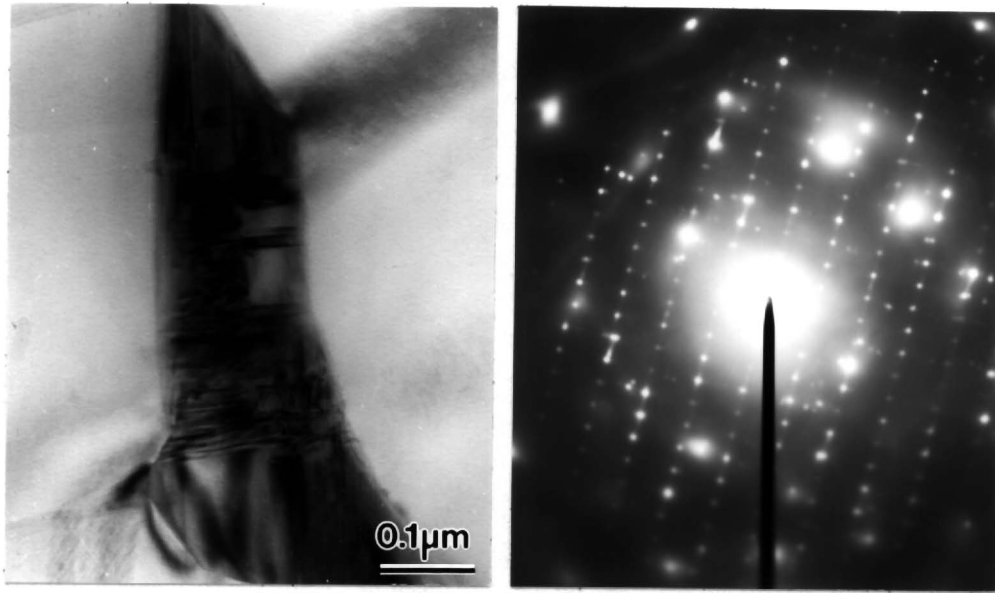
Figure 13: TEM photomicrographs of the specimen exposed at 927°C for 15 minutes in the hot worked condition. Faulted σ phase precipitates and selected area diffraction pattern of σ in <001> zone axis are shown.
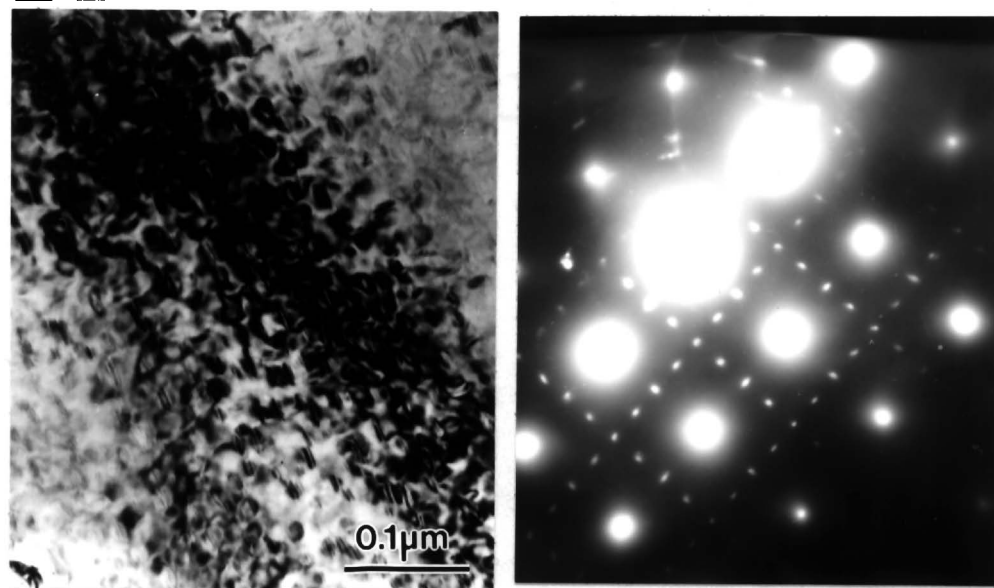

Figure 14: TEM photomicrographs of the specimen annealed at 1149°C for 2h exposed at 760°C for 12h. The γ'/γ" precipitates and selected area diffraction of γ" in <001> zone axis are shown.

Time - Temperature -Transformation Diagram:

Based on the metallographic analyses and hardness, a TTT diagram for alloy 725 is presented in Figure 16. Change in hardness (Figure 1) correlates well with the precipitation. Peak in precipitation kinetics for γ'/γ" occurs at 760°C/816°C which results an increase in hardness of over 300 Vickers Hardness Number in 5-6 hours exposure. At 871°C, γ'/γ" tends to overage resulting in lower hardness than 816°C. Presence of inter and intragranular η on at 927°C exposure does not harden the material. $M_{23}C_6/M_6C$ carbides were detected at the grain boundaries in the temperature range of 704°C to 871°C.
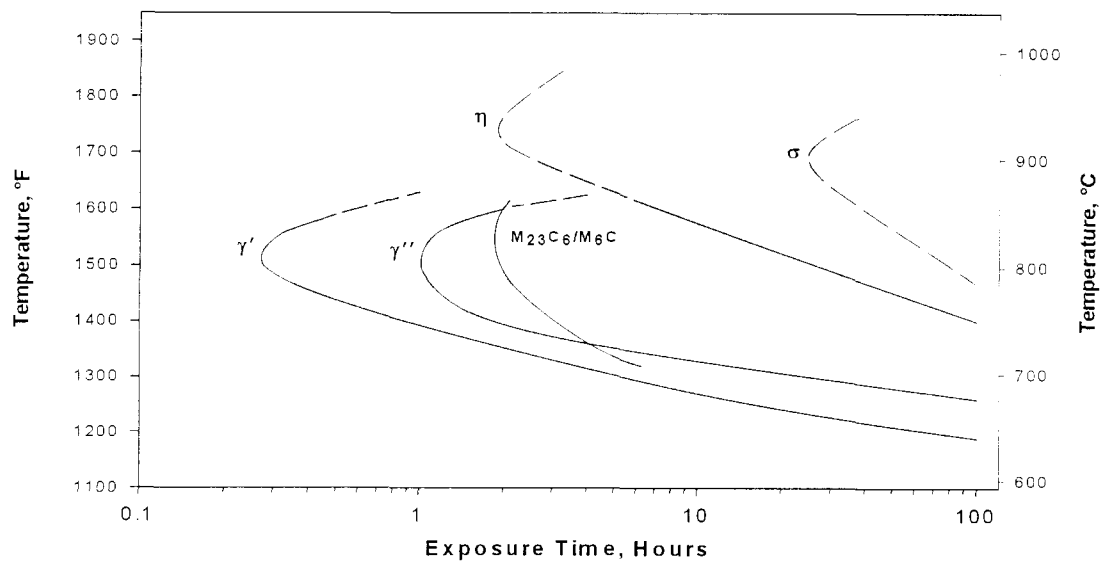
Figure 15: Time – Temperature – Diagram of alloy 725 annealed at 1149°C for 2h based on optical microscopy, SEM, XRD, TEM, and hardness. The dotted lines indicate uncertainty in the exact location of the phase field.

Precipitated Phases:

Gamma Prime: Gamma prime is a $Ni_3(AlTi)$ type phase. It has good solubility for Co, Cr, Fe, Nb, Mo and other elements [7]. Morphology of γ' is related to lattice mismatch between γ' and γ matrix. Gamma prime occurs as spheres at 0-0.2% mismatch, but becomes cubic around 0.5%-1.0%, and then becomes plate like at mismatch above 1.25% [8]. It is ordered face centered cubic $L1_2$ crystal-structure which, contributes anti-phase boundary strengthening to γ-γ' alloys. Lattice parameters of γ-γ' determined by XRD were 3.61A and 3.62A respectively. These lattice parameters are comparable to γ-γ' lattice parameters of alloy 718 reported in the literature [9]. Solvus temperature of γ' in this study was is in the range of 871°C to 927°C. In alloys containing sufficient amount of Ti and Nb, γ' transforms to Ni_3X-type (η/δ) compounds [8]

Gamma Double Prime: Gamma double prime is $Ni_3(NbAlTi)$ type phase. Similar to γ', γ'' also has good solubility for many other elements [7]. It has ordered tetragonal DO_{22} crystal structure. This phase precipitates coherently in the matrix. Lattice parameters, a = 3.62 and c = 7.40, were determined by XRD analysis. Being a metastable phase, γ'' in alloy 725 is likely to transform to η/σ phases. Solvus temperature of γ'' in this study was is in the range of 871°C to 927°C.

Eta Phase: Eta is Ni_3Ti type phase. It has ordered hexagonal DO_{24} crystal structure. It forms on the grain boundaries and in the matrix as isolated platelets or in the form of cellular colonies. Eta has low solubility for Cr and Mo [10]. As η platelets grow they reject these elements into the matrix. Due to low diffusion rate of Cr and Mo this rejection could have created enrichment of these elements adjacent to η platelet resulting in the precipitation of σ phase. Co-precipitation of η/σ is shown in Figure 16. Eta phase in this study was detected on 760°C/100h exposure and on exposure at higher temperatures. Solvus temperature was in the range of 982°C to 1038°C. Although there is good probability for the precipitation of Ni_3Nb type orthorhombic δ phase since alloy 725 contains 3.5 wt% Nb, δ phase was not conclusively isolated in this study.
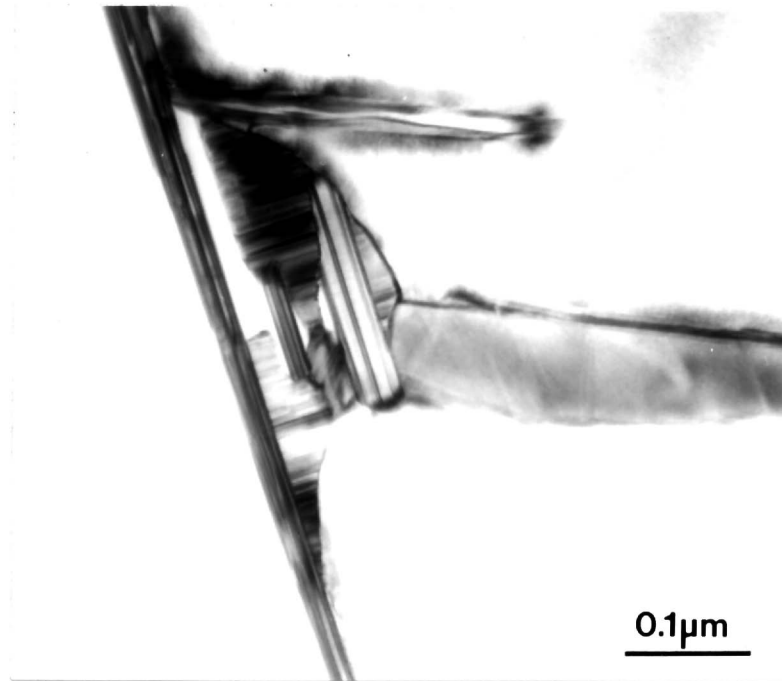
Figure 16: TEM photomicrograph of the specimen hot worked and exposed at 927°C for 15 minutes.

Sigma phase: Sigma phase has a tetragonal $D8_b$ crystal structure. The chemical composition of Sigma determined from the extracted residue by semi-quantitatively SEM/EDX analysis was $Ni_{0.37}Cr_{0.43}Mo_{0.11}Fe_{0.08}Ti_{0.01}$. XRD confirmed that lattice parameters, a = 8.95A and c = 4.62A. Due to its complex crystal structure and generally harmful morphology, σ phase formation can cause marked room temperature and elevated temperature embrittlement. The degree of embrittlement is influenced by the amount and distribution of the phase. Hard acicular precipitates act as an excellent source for crack initiation and propagation. However, a more grave concern is degradation of elevated temperature rupture strength [8]. Sigma contains a high refractory metal content sapped from the matrix of a superalloy, which results in decrease in solid solution strengthening [8].

Conclusions

Alloy 725 is precipitation hardened by γ'/γ'' phases. Ni_3Ti-type η phase is formed at higher temperatures which, transforms to σ phase on prolonged exposure. Residual work expedites σ phase formation. In addition to these phases, $M_{23}C_6/M_6C$ carbides were detected at the grain boundaries. It should be mentioned that the TTT diagram presented in this paper is exclusive to the given chemical composition, size, and processing. Since residual work affects the transformations, alloy 725 annealed at different temperatures particularly below the η solvus would have relatively different TTT diagrams.

Acknowledgements

References

1. E. L. Hibner, H. W. Sizek, and S. K. Mannan, "Elevated Temperature Tensile and Creep Properties of INCONEL alloy 725", Superalloys 718, 625, 706, and Various Derivatives, Ed. E. A. Loria, (Warrendale, PA: TMS, 1997), 491-501.

2. S. K. Mannan, S. J. Patel, J. Dong, and X. Xie, "Crack Growth and High Temperature Thermal Stability of INCONEL alloy 725", Intermetallics and Superalloys, EUROMAT 99, Vol 10, Ed. By D. G. Morris, S. Naka, and P. Caron, WILEY-VCH Weinheim, Germany, 2000, 15-21.

3. E. L. Hibner, "A New Age-Hardenable Corrosion Resistant Alloy for Deep Sour Gas Well Service", Superalloys 718, 625, 706, and Various Derivatives, Ed. E. A. Loria, (Warrendale, PA: TMS, 1991), 895-903.

4. P. Ganessan, E. F. Clatworthy, and J. A. Harris, "Development of a Time –Temperature-Transformation Diagram for Alloy 925", Corrosion, Vol. 44, No 11, 1988, 827-835.

5. K. A. Heck, "The Time- Temperature-Transformation Behavior of Alloy 706", Superalloys 718, 625, 706, and Various Derivatives, Ed. E. A. Loria, (Warrendale , PA: TMS, 1994), 393-404.

6. S. K. Mannan, S. J. Patel, and J. J. deBarbadillo, "Long Term Thermal Stability of INCONEL Alloys 718, 706, 909, and WASPALOY at 593°C and 704°C", Superalloys 2000, Ed. T. M Pollock et al, (PA: Warrendale , PA: TMS, 2000), 449-458.

7. M. G. Bruke, and M. K. miller, "Precipitation in Alloy 718: A combined AEM and APFIM Investigation", Superalloys 718, 625, 706, and Various Derivatives, Ed. E. A. Loria, (Warrendale, PA: TMS, 1991), 337-350.

8. C. T. Sims, N. S. Stoloff, and W. C. Hagel, Superalloys II, (John Wiley & Sons, New York, 1987), 105.

9. M. Prager, and C. S. Shira, "Welding of Precipitation–Hardening Nickel–Base Alloys", Welding Research Council Bulletin # 128, February 1968.

10. S. T. Wlodek, "The Stability of Superalloys", Long Term Stability of High Temperature Materials, Ed. G. E. Fuchs, K. A. Dannemann, and T. C. Deragon, (Warrendale, PA: TMS, 1999).